

# A Catalog of Cosmic Ray Detections in Gaia CCDs

Prepared by : Christian Kirsch (and Asier Abreu) (ESAC)

February 19, 2018

Document Version : v1.0

## Contents

|          |  |           |
|----------|--|-----------|
| <b>1</b> | <b>Objective</b>                               | <b>3</b>  |
| <b>2</b> | <b>Background</b>                              | <b>3</b>  |
| 2.1      | Intro . . . . .                                | 3         |
| 2.2      | Acronyms . . . . .                             | 3         |
| 2.3      | Conventions . . . . .                          | 4         |
| 2.3.1    | Definitions . . . . .                          | 4         |
| 2.3.2    | Reference System . . . . .                     | 4         |
| 2.4      | Data Source . . . . .                          | 4         |
| <b>3</b> | <b>Algorithm Description</b>                   | <b>5</b>  |
| 3.1      | Feature Extraction . . . . .                   | 5         |
| 3.1.1    | SM-SIF: Laplacian Edge Detection . . . . .     | 7         |
| 3.1.2    | BAM-OBS: Boxcar filtering / Stacking . . . . . | 9         |
| 3.1.3    | BAM-SIF: Thresholding . . . . .                | 12        |
| 3.1.4    | Extraction Pipeline . . . . .                  | 14        |
| 3.2      | Post-Processing . . . . .                      | 14        |
| 3.2.1    | Observed Flux . . . . .                        | 14        |
| 3.2.2    | Track Geometries . . . . .                     | 17        |
| 3.2.3    | Flagging Special Tracks . . . . .              | 17        |
| 3.2.4    | Post-Processing Pipeline . . . . .             | 17        |
| <b>4</b> | <b>Data Model</b>                              | <b>17</b> |
| 4.1      | Data Model Description . . . . .               | 17        |
| 4.2      | Event Track Reconstruction . . . . .           | 17        |
| <b>5</b> | <b>Persistence Considerations</b>              | <b>18</b> |

|          |   |           |
|----------|---|-----------|
| 5.1      | Persistence Method(s)                       | 18        |
| 5.2      | Size Estimations                            | 18        |
| 5.3      | Long Term Preservation                      | 19        |
| <b>6</b> | <b>Quality Control Metrics</b>              | <b>19</b> |
| 6.1      | Internal Consistency Checks                 | 19        |
| 6.2      | External Consistency Checks                 | 19        |
| <b>7</b> | <b>Catalog Release Mechanism</b>            | <b>19</b> |
| 7.1      | Catalog Version Generation                  | 19        |
| 7.2      | Release Mechanism and Notification to Users | 19        |

## History of versions

| Version | Date       | Author(s) | Changes                              |
|---------|------------|-----------|--------------------------------------|
| 1.0     | 29.10.2017 | A. Abreu  | First Data Model. Initial Definition |

# 1 Objective

This document describes in detail a relational data model for a catalog of cosmic rays as detected in the Gaia CCDs.

## 2 Background

### 2.1 Intro

The Gaia cosmic rays catalog is the main output product of particle event detection processing performed at ESAC. This off-line processing is aimed to generate a catalogue of cosmic rays that allows to analyze the long term behavior of the radiation environment at L2 as seen by Gaia.

### 2.2 Acronyms

|      |   |
|------|---|
| AC   | Across Scan                             |
| AL   | Along Scan                              |
| AF   | Astrometric Field                       |
| SM   | Sky Mapper                              |
| BAM  | Basic-Angle Monitoring device           |
| CCD  | Charge-Coupled Device                   |
| TDI  | Time Delay Integration                  |
| SIF  | Service Interface Function              |
| FITS | Flexible Image Transport System         |
| FoV  | Field of View                           |
| FPA  | Focal-Plane Assembly                    |
| OBMT | On-Board Mission Time                   |
| UTC  | Coordinated Universal Time              |
| °    | degree; unit of angle                   |
| '    | arcminute, minute of arc; unit of angle |
| ''   | arcsecond, second of arc; unit of angle |

## 2.3 Conventions

The following set of definitions and conventions are simply a subset of those (thoroughly) defined in [1]. We have adopted those referring to CCD characteristics and relevant for the present scope.

### 2.3.1 Definitions

- A ‘pixel’ is the elementary charge generation and storage element in the light-sensitive area of the CCD.
- A ‘column’ is the set of all pixels having the same across-scan coordinate.
- A ‘line’ is the set of all pixels having the same along-scan coordinate.
- The ‘summing register’ is a special pixel line following the light-sensitive pixels. It is used to combine (add or bin) the charges from several lines into one.
- The ‘read-out register’ is the special pixel line which is used to transfer the accumulated charges from the CCD chip into the read-out amplifier (and thus further into the further amplification and digitisation electronics).
- The ‘read-out amplifier’ is the electronic circuit at the end of the read-out register where the registration and pre-amplification of the photoelectric charges takes place.
- The ‘time delay integration’ mode (TDI mode) consists of gradually shifting the photoelectric charges from “left” to “right” — and eventually into the read-out register — to follow moving optical images over the light-sensitive area.
- ‘Gates’ are special lines within the light-sensitive area. If activated they act like summing registers, holding up charges, preventing them from moving along scan in spite of the TDI clocking. This causes a compression (summing) of the already accumulated TDI images into a single line, and the creation of a new “blank” empty space “in front of” this line.

*It would be nice here to add a latex native graphics of the CCD sumarizing all this*

### 2.3.2 Reference System

Certainly needed.

The following image shows the Gaia Focal Plan Array composed of 106 CCDs and the different CCD variants (BAM/AF):

*It would be nice here to add here a latex native graphics of the FPA*

## 2.4 Data Source

For the analysis of the cosmic rays in Gaia CCDs we have used a number of different *engineering* datasets. Namely:

- Sky Mapper images downlinked via the Service Interface Function - from here on shortened to SM-SIF. These images are recorded fully in TDI mode and contain objects of interest such as planets, comets, dense stellar fields such as globular clusters or the Galactic center as well as, most frequently, very bright stars that drive the CCDs into saturation.
- Nominal BAM observations, from here on shortened to BAM-OBS. These images consist of two readout windows roughly  $1 \times 1$  cm in size located on one chip, which continuously observe the interference pattern of the BAM in staring mode.
- SIF BAM observations, shortened to BAM-SIF. These images record the same AC region as the BAM-OBS source images, but span the width of the entire chip in AL. They thus contain off-pattern regions with a very weak background. This dataset has been previously analyzed for cosmics in [2].

### 3 Algorithm Description

A number of different event detection algorithms have been used for the generation of the catalog. Each algorithm is tailored to the Gaia detector type. Where possible, existing algorithms for cosmic ray detection in CCDs have been used. The following subsections briefly describe the types of algorithms used.

The extraction of the data product has been split into two steps, a feature extraction and a post-processing. The first step uses the input of the different data sources to produce for every observation a list of objects that have been recognized as cosmic ray tracks. The second step then analyzes the extracted tracks further, adding information such as their orientation on the FPA or their length.

#### 3.1 Feature Extraction

The goal of the feature extraction step is to collect all the objects recognized as cosmic ray tracks from the different datasets into a source-independent dataset for the post-processing. To that extent, we have defined an intermediary dataset named TrackObs (short for track observation), which collects necessary metadata on the source observation and contains a list of all identified objects.

Each TrackObs contains a list of metadata on the source observation, including:

- Source observation (SM-SIF, BAM-OBS, BAM-SIF)
- Acquisition time in OBMT
- Source image dimension (in AL and AC)
- Number of pixels not used for extracting cosmics (for the calculation of the exposed area)
- Sample binning, in AL and AC
- CCD gain
- Chip location on the FPA (Row and FOV)

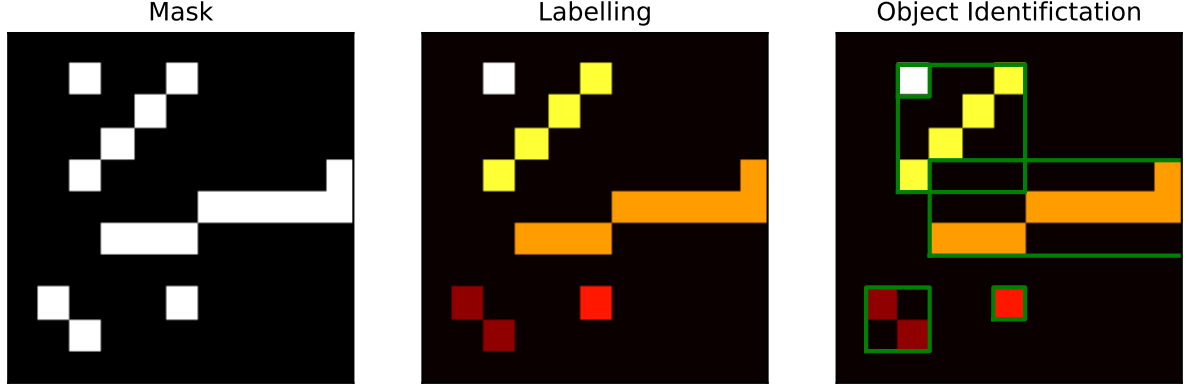


Figure 1: Identification of individual connected objects from a cosmic ray mask. The boolean mask (left panel) is used to calculate an integer array for all 8-connected pixels, which are labeled with a unique integer per object (middle panel). Objects are then identified by their labels as rectangular image sections around all pixels with a common label (green boxes in right panel).

The output of all of the following algorithms are three two-dimensional arrays of the same size as the input image: A boolean mask array set to True for all pixels identified as cosmics, a signal array consisting of the original image minus the non-cosmic 'background', and an array of the uncertainty of this signal array. As the conversion of these arrays into cosmic ray tracks is the same in all of the following algorithms, we will explain the process here.

First, individual objects are identified from the mask. This process is shown in Figure 1. From the boolean mask, a labelling algorithm from the `scipy` Python distribution is used to assign the same integer value to all neighbouring pixels set to True – in this case, if they are horizontally, vertically or diagonally adjacent. The labelled array is then used by a `scipy` object finding algorithm to identify the bounding boxes of all pixels of the same label.

Each `TrackObs` then contains an array whose rows represent information on one of the objects identified in the above steps. For each track, it lists:

- The AL and AC lengths of the bounding box
- The location of the track, encoded as the lowest AL and AC value in its bounding box
- The sub-image of the track from the signal array, encoded in ADU. Note that this only includes those pixels inside the bounding box with the corresponding label - in the right panel of Fig. 1, the image of the  $4 \times 4$  diagonal track in the upper left does not include the single pixel track in its bounding box, which has a different label.
- The sum of signal values of the track in electrons, corresponding to the total measured ionizing energy.
- The uncertainty of the total ionizing energy, being the square root of the sum of the squares of the individual pixel uncertainties.

Each of the following algorithms produces such `TrackObs` objects, which are saved intermediately as FITS files.

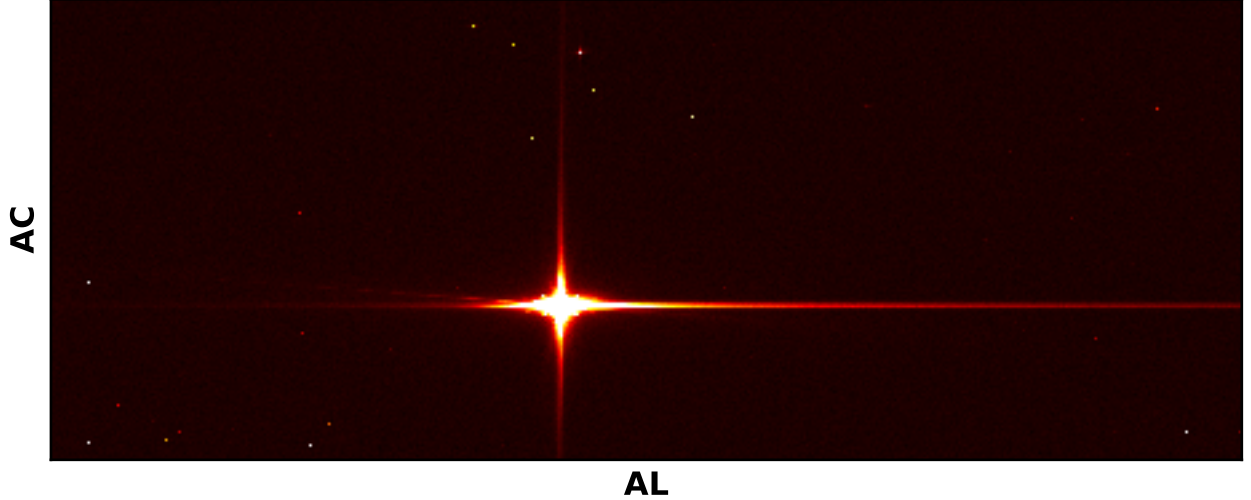


Figure 2: An example of a SM-SIF source image. Axis orientation is the standard Gaia convention, with the serial register to the right and readout to the upper right corner. The aspect ratio has not been corrected for pixel geometry and binning.

### 3.1.1 SM-SIF: Laplacian Edge Detection

Figure 2 demonstrates a typical image in the SM-SIF dataset. The image contains a bright star object with a PSF that contains long diffraction spikes and a saturated core. Smaller stars and what appear to be cosmic ray tracks can be detected by bare eye.

To automate the detection of cosmic ray tracks in these images, they must be successfully separated from the imaged astronomical objects. Such algorithms, usually used to remove unwanted cosmic rays, have been developed for earlier ground- and space-based observatories and can be used in to our advantage. For this dataset, we decided to utilize the L.A. COSMIC algorithm described in [3]. Briefly summarized, this algorithm utilizes a variation of Laplacian edge detection to discriminate cosmic ray tracks from stars by their sharp edges, which separates them from the smoother PSFs of stars.

In more detail, the algorithm first convolves a subsampled version of the original image with a derivative filter, which assigns high values to sharp edges. The resulting image is compared with a noise image, calculated by a  $5 \times 5$  median filter of the image and including the CCD readout noise. Pixels with a signal-to-noise-ratio above a high threshold are then selected as first candidates for noise pixels, after which a lower threshold is applied to neighbouring pixels. The identified pixels are then masked and the original image is cleaned, replacing the cosmic ray pixels with the median or mean of the surrounding, unmasked pixels. This procedure, starting from the convolution, is applied iteratively until either no more pixels are identified or the maximum number of iterations has been reached.

This analysis utilizes a Python implementation of the L.A. COSMIC algorithm called ASTRO-SCRAPPY [4] for cosmic ray identification.

First attempts at simply applying ASTRO-SCRAPPY to images like the one in Fig. 2 revealed that the bright stars in most of the SM-SIF images were still falsely detected as cosemics. The reason for this is their saturation of the detector – see especially the middle panel of Figure 3. The bright star, as it saturates the detector, causes a strong blooming effect, saturating even

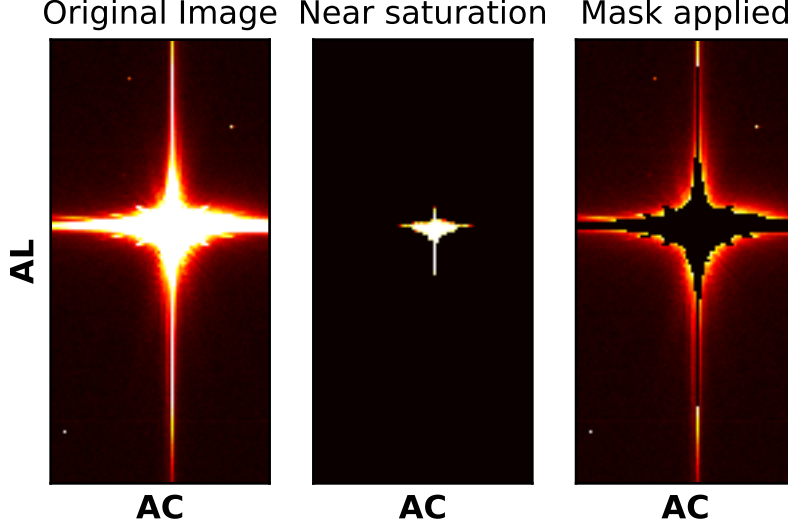


Figure 3: Bright stars in SM-SIF and their masking. *Left:* The appearance of the bright star from Fig. 2. *Middle:* The left panel after applying a high threshold. The bright pixels are fully saturated and show a sharp charge transfer pattern. *Right:* The left panel after applying bright star filtering - the core and a large part of the diffraction spikes are masked.

the pixels read in after those exposed to the bright stars (the image read out direction is to the top). As the panel shows, the resulting pattern has a very sharp gradient, which is picked up by the Laplacian filter and mis-identified as a cosmic.

To eliminate these bright star cores and mask their extended field, in which cosmics will disappear under the poisson noise of the star, we apply a simple algorithm before extracting cosmics. Its steps are:

1. Object finding: Construct a mask set to 1 for every pixel above a low threshold and apply object labelling to this mask. This step essentially catches all stars and cosmics.
2. Saturated object identification: Of all objects, select only those that contain at least one pixel at a value of 65535 ADU, the maximum of a 16-bit integer.
3. Masking: Add all the objects identified in the previous steps to a mask (set to 1 for invalid pixels). This mask can be forwarded to ASTRO-SCRAPPY, which supports masked regions and does not use them for cosmic identification.

The results of this algorithm can be seen in the right panel of Fig. 3, where all pixels belonging to the bright star are set to zero. There still remain some parts of the bright star's PSF - these, however, are very close to the bias level and decay smoothly, thus causing no issues.

Using the bright star removal, we then constructed the following algorithm to extract cosmics from SM-SIF observations:

1. Read in the image and construct the bright star mask.
2. Subtract the AL-dependent bias and apply the gain-scale, as L.A. COSMIC requires an image in units of electrons to calculate the Poisson noise.



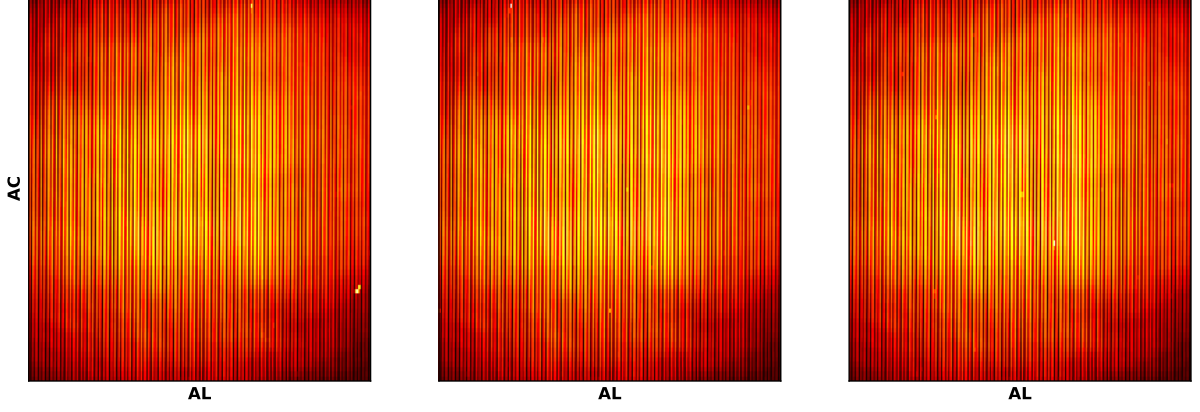


Figure 4: A series of three BamObservations from FOV 1. The dimensions have been rescaled to the physical dimension of the CCD – each image pixel represents a  $10 \times 120 \mu m$  ( $AL \times AC$ ) sample. Individual pixels that deviate from the patterns can be recognized as cosmic ray tracks.

3. Apply L.A. COSMIC, which returns the cosmic ray mask and a cleaned image. The values of the cleaned image are calculated by taking the mean of the surrounding, non masked pixels in a  $5 \times 5$  pixel area, i.e. for a pixel located at  $(AL, AC)$ , the cleaned value is

$$\text{Clean}(AL, AC) = \left( \sum_{\substack{\text{mask=False} \\ AL-2 \leq i \leq AL+2 \\ AC-2 \leq j \leq AC+2}} \text{Source}(i, j) \right) / \left( \sum_{\substack{\text{mask=False} \\ AL-2 \leq i \leq AL+2 \\ AC-2 \leq j \leq AC+2}} 1 \right)$$

4. Calculate the signal array as  $\text{Signal}(AL, AC) = \text{Source}(AL, AC) - \text{Clean}(AL, AC)$
5. Calculate the uncertainty array as the square root of the variance of the signal array, calculated as

$$\text{Var}(AL, AC) = \text{Source}(AL, AC) + \sigma_{\text{rn}}^2 + \sum_{\substack{\text{mask=False} \\ AL-2 \leq i \leq AL+2 \\ AC-2 \leq j \leq AC+2}} \frac{\text{Source}(i, j) + \sigma_{\text{rn}}^2}{N_{\text{mean}}(AL, AC)},$$

with  $\sigma_{\text{rn}}^2$  denoting the pixel readnoise, and  $N_{\text{mean}}(AL, AC)$  denoting the number of pixels used to calculate the mean for cleaning this pixel. As one can see from the equation, the noise of the source image has been assumed to be Poissonian noise and readnoise.

6. Extract tracks from the mask, signal and uncertainty images and save them as a TrackObs, as described above.

### 3.1.2 BAM-OBS: Boxcar filtering / Stacking

Figure 4 shows a series of observations from FOV 1 of the BAM. The three images were recorded in series (left to right) with an exposure time of about 23 seconds each. It is visibly apparent that the BAM patterns do not significantly between single observations, yet all three images contain pixels deviating from the pattern that only exist in one given image. These spurious pixels are a clear sign of cosmic rays.

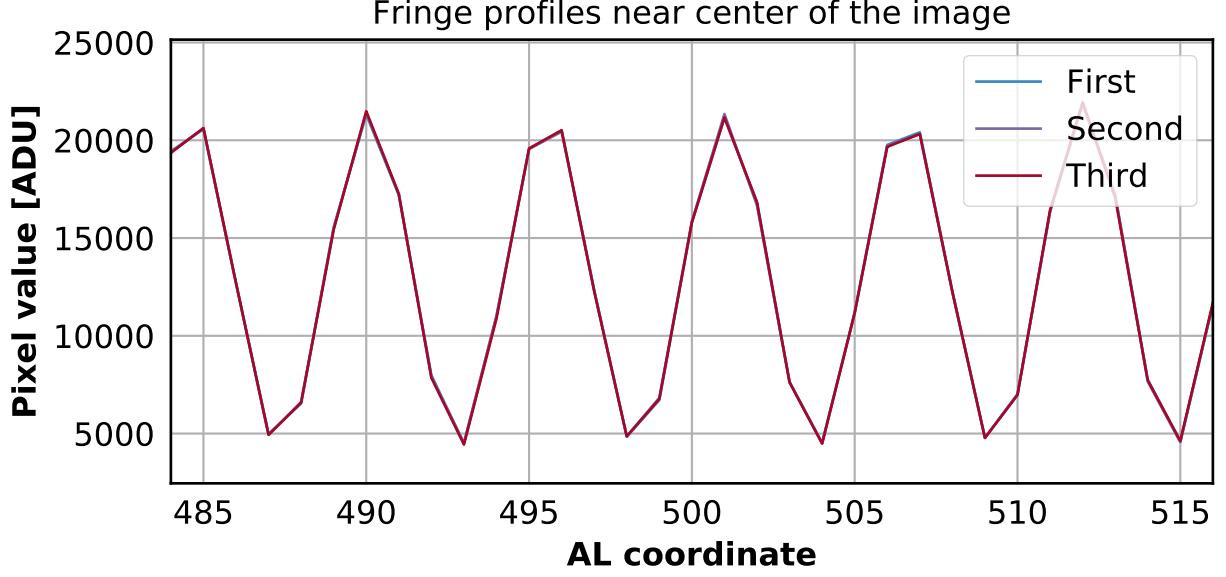


Figure 5: The ADU values of the three patterns in Fig. 4 plotted along the center of the images in AC across a narrow AL region in the center. The interference pattern is very sharp, with a period of about 5 pixels in AL. The fringes of all three images overlap very closely.

Figure 4 further demonstrates that the interference pattern does not vary aside from Poissonian noise between the three images. It also shows why a simple application of the L.A. COSMIC algorithm to this dataset will immediately fail: The interference patterns themselves are very sharp, with a peak-to-trough distance of about 2 to 3 pixels. The algorithm is totally blinded by the pattern and can not separate it from the cosemics.

For our track extraction algorithm, we exploited the fact that the interference pattern is relatively static. In astronomy, multiple exposures of the same object (assuming constant luminosity) are used to reject the spurious high pixel values caused by cosmic rays – a similar algorithm is used to reject cosemics in BamObservations when analyzing the pattern. In our case, we can simply do the reverse, and accept pixels that vary significantly stronger than the inherent counting and readout noise as the tracks of cosmic rays.

The concrete algorithm assumes as an input a time-ordered series of BamObservations from a single FOV, and operates on a range of observations, which we refer to as a BoxCar. To create a good estimate of the pattern across a period of time where it does not vary, we chose to use a total of 7 images at once - a central image for cosmic ray extraction and the three images recorded immediately after and before. The extraction algorithm works as follows.

1. Construct the BoxCar: Read the first 7 BamObservations – applying the electron conversion gain – into a three dimensional array with the indices  $t$ ,  $AL$  and  $AC$  - with  $t \in [1, \dots, 7]$  ( $t = 3$  being the central observation), and  $AL$  and  $AC$  denoting the image dimensions.
2. Sigma-clipping: Compute the median and standard deviation across time and mark all the pixels whose difference to the median exceeds a chosen threshold - these are likely cosemics, and will not be used to calculate the pattern.
3. Calculate a two-dimensional image array of the pattern, by taking the mean across time

without using the sigma-clipped pixels, e.g.

$$\text{Pattern}(AL, AC) = \left( \sum_{t \text{ not clipped}} \text{BoxCar}(t, AL, AC) \right) / \left( \sum_{t \text{ not clipped}} 1 \right).$$

4. Calculate the signal array by subtracting the Pattern from the central array in the BoxCar, e.g.

$$\text{Signal}(AL, AC) = \text{BoxCar}(t = 3, AL, AC) - \text{Pattern}(AL, AC).$$

5. Calculate the uncertainty array as the square root of the variance of the signal array, calculated as

$$\text{Var}(AL, AC) = \text{BoxCar}(t = 3, AL, AC) + \sigma_{\text{rn}}^2 + \sum_{t \text{ not clipped}} \frac{\text{Boxcar}(t, AL, AC) + \sigma_{\text{rn}}^2}{N_{\text{mean}}(AL, AC)},$$

with  $\sigma_{\text{rn}}^2$  denoting the pixel readnoise, and  $N_{\text{mean}}(AL, AC)$  denoting the number of pixels in the BoxCar that have not been rejected by sigma clipping at this  $(AL, AC)$  pair. As one can see from the equation, the noise of the BamObservations has been assumed to be Poissonian noise and readnoise.

6. Create the cosmic mask: Divide the signal array by the uncertainty array and create the boolean mask array, set to true where the signal/uncertainty ratio is greater than a threshold  $f$ . Due to the strong photon background, some cosmic pixels are missed in this step. We attempt to mitigate this by investigating all the pixels that neighbour the previously masked pixels, found via binary dilation, and applying for them a signal/uncertainty threshold of  $r_{\text{Neighbour}} * f$ , adding the pixels that satisfy this condition to the mask as well.
7. Apply a track connection algorithm: Even after the previous step, visually apparent long cosmic ray tracks still remain separated - refer to the left panel of Figure 6 for an illustration. Tracks that are oriented in the AL direction see a strongly variable photon background, seen as fluctuations in the uncertainty array. These pixels are less likely to be detected by the thresholding of before. Especially towards the center of the image, where the pattern amplitude is very high, this leads to a single, long cosmic being detected as multiple short cosemics in the troughs of the interference pattern, which eventually leads to an overestimation of the cosmic ray rate.

In an attempt to correct for this track separation, we implemented a track connection algorithm: We first apply to the mask an 8-connected binary dilation followed by a 4-connected binary erosion (this is a variant on binary closing, which uses the same structuring elements for the dilation and erosion instead), illustrated in the middle and right panels of Fig. 6. As the Figure shows, this marks several pixels of interest that may connect the separated objects.

We then examine each of the newly merged tracks, which are identified by the standard labelling algorithm. For each of the tracks, we first calculate the mean of the previously identified signal pixels of this track,  $m_{\text{Object}}$ . Assuming that a cosmic ray creating a long track should have a constant energy deposition per path length, we examine each of the candidate pixels (at the location  $(AL, AC)$ ), checking for the condition

$$|\text{Signal}(AL, AC) - m_{\text{Object}}| > cfac * \sqrt{\text{Var}(AL, AC)},$$

with  $cfac$  being an algorithm parameter. The above equation checks whether the signal value of the candidate pixel is sufficiently close to the value of the other pixels in this object. If a pixel satisfies the condition, it is added to the pixel mask.

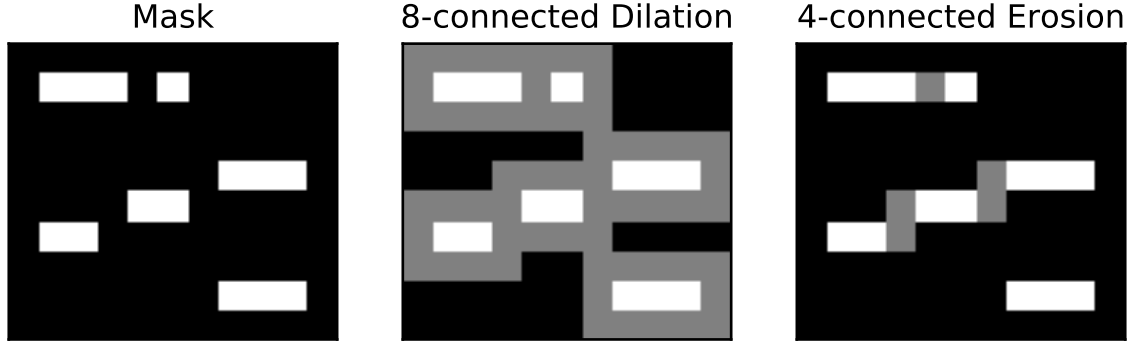


Figure 6: Illustration of the track connection algorithm used for this dataset. *Left:* An example of a cosmic ray mask where ray tracks oriented in the AL direction have not been fully identified. *Middle:* Application of 8-connected binary dilation to the mask - the added pixels are shown in gray. *Right:* Additional application of 4-connected binary erosion, shown in the gray pixels, which are examined by the connection algorithm.

8. Extract tracks from the mask, signal and uncertainty images and save them as a TrackObs, as in SM-SIF and described above.
9. Update BoxCar: Read in the next BamObservation and replace the oldest pattern in the BoxCar with it – the BoxCar is utilized as a FIFO, in this case. We then update the central pixel index and repeat starting step 2 until all BamObservations have been processed.

### 3.1.3 BAM-SIF: Thresholding

Figure 7 depicts an example for a BAM-SIF image used in this extraction. These images both contain the interference pattern in the BAM-OBS images, as well as off-pattern regions showing the TDI footprint of the pattern, which is only AC-dependent. These images are much less frequently sampled than the BAM-OBS images – usually a handful of images twice per week – which is why they are not very useful for the purpose of particle monitors. However, the off-pattern regions offer a good opportunity to extract cosmic rays from the BAM chip with a much lower and simpler background than that of BAM-OBS, allowing us to examine the effect the pattern has on the above extraction.

As this dataset is very attractive for cosmic ray extraction, it has been used before for cosmic ray studies, see [2]. This algorithm builds on the previous extraction, merging it into the TrackObs-based files approach utilized here.

For the extraction of cosmic rays, we utilize the two regions outlined in blue and green boxes in Fig. 7. A smaller region in AC has been selected for the FOV 1 region - the ignored region has shown a high stray light contamination, which causes mis-identifications.

The extraction algorithm for this dataset is then (for each region separately):

1. Read in the image and apply the gain scale.
2. Determine the AC-dependent TDI background: Take the 99 columns with the highest AL value (to the left in Fig. 7) and remove the outliers – for each column within, discard

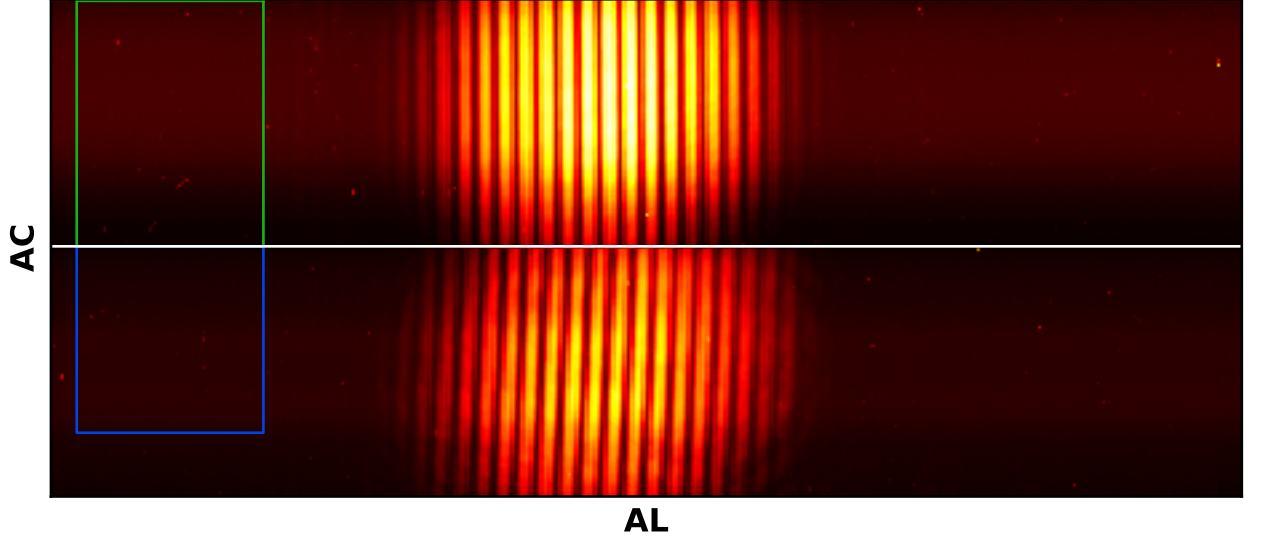


Figure 7: An example of a BAM-SIF source image, which has been rescaled to the physical CCD dimensions. The top half of the image shows the AC region of FOV 2, the bottom half that of FOV 1. The off-pattern regions in green and blue boxes are used for cosmic extraction.

the highest and lowest 25 % of pixel values to remove cosmics. Then, calculate the mean and standard deviation of the remaining image pixels for each line. The output are two one-dimensional arrays of the AC-dependent TDI background and its standard deviation.

The removal of the TDI background is demonstrated in Figure 8

3. Calculate the signal and variance arrays as

$$Signal(AL, AC) = Source(AL, AC) - Background(AC)$$

and

$$Var(AL, AC) = Source(AL, AC) + \sigma_{rn} + \sigma_{Background},$$

with  $\sigma_{rn}$  being the readnoise and once again assuming Poisson noise in the source array. The uncertainty array is then the square root of the variance array.

4. Construct the mask array in exactly the same way as for BAM-OBS, including the track connection. While this should not be necessary here, we want to have as similar as possible algorithms for BAM-OBS and BAM-SIF, to see the effect of the pattern.
5. Extract tracks from the mask, signal and uncertainty images and save them as a TrackObs, as in the algorithms above.

All steps until the calculation of the signal are the same as in [2], which only returned the signal images.

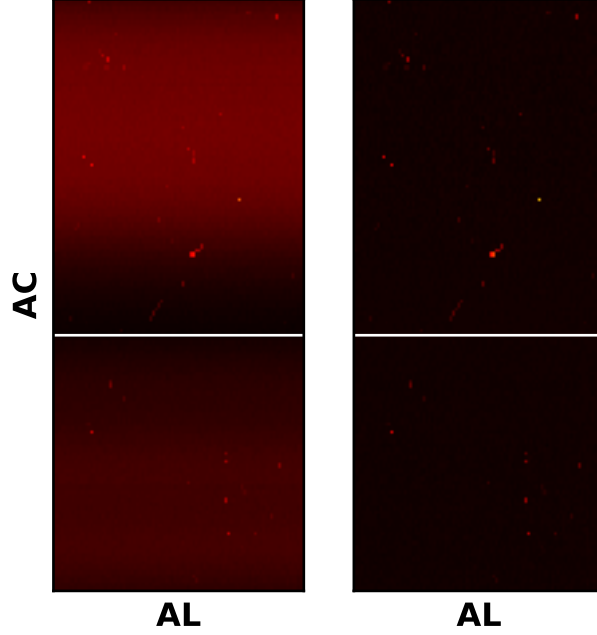


Figure 8: *Left*: The two extraction regions from Fig. 7. *Right*: The same image with the TDI background removed, leaving only cosmic ray tracks.

### 3.1.4 Extraction Pipeline

## 3.2 Post-Processing

### 3.2.1 Observed Flux

One of the first – and most simple – data products that can be derived from a TrackObs is the flux measured per observation. The calculation of a flux is in this case very simple: Given an exposed CCD area  $A_{\text{exp}}$  and exposure time  $T_{\text{exp}}$  the flux is simply calculated as

$$F = \frac{\text{Counts}}{A_{\text{exp}} \cdot T_{\text{exp}}}$$

In the following, we determine these values for SM-SIF and BAM observations, whose computation are not trivial due to the use of TDI (and in the latter case, staring) observations and the size of the used AL readout windows relative to the physical CCD size.

For our calculations: A Gaia CCD is segmented into 4500 pixels in AL direction and 1980 pixels in AC direction - of these, 14 pixels are in the pre-scan region and not used. Pixels are  $10 \times 30 \mu\text{m}$  (AL  $\times$  AC) and TDI transfer time is  $T_{\text{TDI}} = 0.9828 \text{ ms/pixel}$ , so the effective CCD exposure time is 4.4226 s.

### SM-SIF

The readout of the SM-SIF images are a continuous readout of the signal acquired from TDI (see also Fig. 9). To avoid saturation from bright stars, Gate 12 is permanently activated, leading to a readout of only the last 2900 CCD lines in AL. Pixels are then binned to a factor of 2 in both AL and AC.

# TIKZ PLACEHOLDER

Figure 9: Scheme of an SM acquisition. The CCD area of each chip after Gate 12 is continuously read out via TDI (left). The resulting image (right) has the same dimension in AC but a dimension in AL dependent on the duration of the readout.

For clarity in notation, I will, from now on, use the following terms:

- A **CCD pixel** refers to a physical pixel on the actual CCD - i.e. one physical unit of  $10 \times 30 \mu\text{m}$
- An **image pixel** refers to a pixel in the image recorded after the TDI scan. While it still carries spatial information in AC, its AL information is a result of the integration over the sampled region in AL - it encodes time and location. Thus, an image pixel does not correspond to a single physical pixel, but rather the history of an entire AL line during TDI.

The resulting image, then, consists of 983 image pixels in AC and a variable number  $N_{\text{AL}}$  of image pixels in AL - depending on the time over which data has been recorded (which is  $T_{\text{rec}} = T_{\text{TDI}} \cdot 2N_{\text{AL}}$ ).

From a physical pixel perspective, each CCD pixel has been exposed for the time  $T_{\text{rec}}$ , with the information of individual exposures spread over different image pixels in AL. The exposed area corresponds to that of  $2900 \times 1966$  physical pixels.

From an image pixel perspective, each pixel has been exposed for exactly  $T_{\text{TDI}} \cdot 2900$ , regardless of  $N_{\text{AL}}$ . The physical area of each image pixel corresponds to that of 4 physical pixels, due to binning.

As one can tell from the above, the physical perspective has a lower number of pixels, but a higher exposure time per pixel (assuming  $2N_{\text{AL}} > 2900$ ). The image perspective has more pixels, but lower exposure times. Irregardless of the perspective, the product  $A_{\text{exp}} \cdot T_{\text{exp}}$  - which is of interest for computing fluxes - is always the same, being

$$\begin{aligned} \text{Physical : } A_{\text{exp}} \cdot T_{\text{exp}} &= (2900 \cdot 1966 \cdot 10 \mu\text{m} \cdot 30 \mu\text{m}) \cdot (T_{\text{TDI}} \cdot 2N_{\text{AL}}) \\ \text{Image : } A_{\text{exp}} \cdot T_{\text{exp}} &= (N_{\text{AL}} \cdot 893 \cdot 4 \cdot 10 \mu\text{m} \cdot 30 \mu\text{m}) \cdot (T_{\text{TDI}} \cdot 2900) \\ &= 33.62 \left( \frac{N_{\text{AL}}}{1000} \right) \text{ cm}^2 \text{ s} \end{aligned}$$

Going forward, we will use the image perspective, as it is consistent with prior studies of the BAM image and more useful for the next section. It is also, as we'll see later, easier to treat masked pixels. Nevertheless, for the calculation of fluxes, both perspectives are equivalent.

**BAM-OBS and BAM-SIF** For the BamObservations, pixels are binned by a factor of 4 in AC and not binned at all in AL.

The determination of an exposure time in both pictures for the BamObservations is complicated by the fact that it is not only a TDI observation, but also contains a period of staring. Normally, the BAM CCD is operated in TDI mode, in the same way as the SM CCD. To record the

interference pattern, an exception is made – for an integration time of 19 s, the shifting of charges is stopped, and the chip operates in a kind of staring mode. In nominal BamObservations, data is then only acquired from sub-regions of the CCD that have been illuminated by the BAM pattern. BAM-SIF images use the entire CCD in AL direction along a restricted AC range.

## TIKZ PLACEHOLDER

Figure 10: Readout scheme for a BAM pattern in BAM-OBS. BAM fringe patterns are outlined as red circles. a) Create the readout windows. b) Move the readout windows via TDI. c) Stare observation – charges are not shifted. d) Move readout windows via TDI. e) Readout, recording only contents of windows.

The observation principle and the effect on imaging particle tracks is shown in Fig. 10. Effectively, data is collected from two windows, outlined in green and blue. These two windows have an unbinned length of 1000 in AL and 320 in AC each. They first move across the chip, stay in place during the staring, and then move again to the readout register.

In BAM-SIF observations, we can make a similar estimation of the readout window sizes, although the image dimensions are variable. We will from now on use two values  $N_{AL}$  and  $N_{AC}$  to refer to the binned image dimensions of the result image. The used unbinned lengths are then  $N_{AL}$  and  $4 N_{AC}$ , respectively – for reference, a nominal BamObservation has  $N_{AL} = 1000$  and  $N_{AC} = 80$

The exposure can once again be viewed in two pictures, the physical pixel and image pixel based ones. In the former, it is easy to see that the entire region both readout windows cross are exposed – the exposed area is  $4500 \times 4 N_{AC}$  pixels ( $AL \times AC$ ) per pattern. The exposure time, however, is more complex: First, the entire exposed region is exposed for  $N_{AL} \times T_{TDI}$ , due to the movement of the readout windows across the chip. Additionally, the region used for staring is observed for a further 19 s. The exposure time is, as such, AL-dependent.

In the image picture, the calculation is much easier. Viewing each readout window as a physical unit, the exposed area per window is simply  $N_{AL} \times 4 N_{AC}$  pixels. The exposure time is simply the TDI transfer time across the whole chip plus the staring time.

The product of exposed area and exposure time, which is of interest for flux determination, is in both pictures (per readout window)

$$\begin{aligned} \text{Physical : } A_{\text{exp}} \cdot T_{\text{exp}} &= (4500 \cdot 10 \mu m \cdot 4 N_{AC} \cdot 30 \mu m) \cdot (N_{AL} \cdot T_{TDI}) \\ &\quad + (N_{AL} \cdot 10 \mu m \cdot 4 N_{AC} \cdot 30 \mu m) \cdot (19 s) \\ \text{Image : } A_{\text{exp}} \cdot T_{\text{exp}} &= (N_{AL} \cdot 10 \mu m \cdot 4 N_{AC} \cdot 30 \mu m) \cdot (4500 T_{TDI} + 19 s) \\ &= 22.49 \text{ cm}^2 \text{ s} \quad (\text{for BAM-OBS}). \end{aligned}$$

As the computation is more simple in the image picture, we will from now on use this picture.

### Masked Pixels

In both SM and BAM images, some image pixels can not be used for the determination of cosmics. In the SM, these pixels are mostly caused by the bright star masking algorithm. For the BAM, charge overflow effects can be caused by a high energy cosmics coincident with an interference fringe, fully saturating the pixel and causing errors in the readout of several following pixels.



Correcting the exposed area for these masked pixels is very easy in the image picture, as we simply discard these pixels, meaning one can calculate the exposed area using

$$A_{\text{exp}} = (N_{\text{tot}} - N_{\text{mask}}) \cdot b_{\text{AL}} \cdot b_{\text{AC}} \cdot 10 \cdot 30 \mu m^2$$

With  $N_{\text{tot}}$  being the total number of image pixels,  $N_{\text{mask}}$  being the number of masked pixels and  $b_{\text{AL}}$  and  $b_{\text{AC}}$  being the binning factor in AL and AC, respectively.

### 3.2.2 Track Geometries

For Particle tracks covering a significant amount of pixels, it is possible to estimate the the orientation and the length of the particle track for the purposes of future analysis.

### 3.2.3 Flagging Special Tracks

i.e. those at the edge of the readout windows. Maybe also the removal of tracks at obviously too low energies?

### 3.2.4 Post-Processing Pipeline

## 4 Data Model

This data model is composed of entities *CosmicObservation* which are described in full detail in the following subsection.

### 4.1 Data Model Description

**Entity Name:** *CosmicObservation*

**Entity Description:** A table of cosmic ray (prompt particle event) detections from any of the analyzed Gaia CCDs

**Entity Header:**

**Entity Columns:**

### 4.2 Event Track Reconstruction

We should describe here (TBD if needed) a simple way to reconstruct the window for a given detection from the provided data.

| <i>Name</i>      | <i>Description</i>                                    | <i>Unit</i>                                | <i>Type</i> |
|------------------|---|--|-------------|
| SOURCE           | Descriptor of the type of source observation          | NA   | String      |
| CCD_ROW          | CCD row of the source chip                            | NA   | Short       |
| FOV              | FOV of the source chip                                | NA   | Short       |
| ACQTIME          | Source acquisition time                               | OBMT                                       | Integer     |
| SRC_AL           | AL-dimension of the source image                      | pixels                                     | Short       |
| SRC_AC           | AC-dimension of the source image                      | pixels                                     | Short       |
| BINNING ?        | Source binning  |  | Short       |
| MASKPIX          | Number of masked pixels in the source image           | pixels                                     | Short       |
| GAIN ?           | Source image gain                                     | e-/ADU                                     | Float       |
| EST_FLUX         | Estimated particle flux                               | particles cm <sup>-2</sup> s <sup>-1</sup> | Float       |
| EST_FLUX_ERR     | Poisson Uncertainty of estimated particle flux        | particles cm <sup>-2</sup> s <sup>-1</sup> | Float       |
| SC_POS_X         | Spacecraft X position in corotating coordinate system | m  | Float       |
| SC_POS_Y         | Spacecraft Y position in corotating coordinate system | m  | Float       |
| SC_POS_Z         | Spacecraft Z position in corotating coordinate system | m  | Float       |
| SUN_ASPECT_ANGLE | Spacecraft sun aspect angle                           | deg  | Float       |

Table 2: Event detection table header version v1.0

| <i>Name</i>        | <i>Description</i>  | <i>Unit</i>   | <i>Type</i> |
|--------------------|---|---------------|-------------|
| TRACK_START_POS_AL | The start position of the event in the AL direction                         | pixel         | Short       |
| TRACK_START_POS_AC | The start position of the event in the AC direction                         | pixel         | Short       |
| TRACK_DIM_AL       | Event track dimension in AL   | pixel         | Short       |
| TRACK_DIM_AC       | Event track dimension in AC   | pixel         | Short       |
| TRACK_PIX ?        | Number of detected pixels   | pixels        | Short       |
| TRACK_EN           | Event track total energy  | electrons     | Integer     |
| TRACK_EN_ERR       | Uncertainty in the event track total energy                                 | electrons     | Integer     |
| TRACK_TRUNCATED    | Is the event truncated by start/end of CCD physical area                    | NA            | Boolean     |
| EST_TRACK_LEN      | Estimated incident particle track length (if applicable)                    | $\mu\text{m}$ | Float       |
| EST_TRACK_LEN_ERR  | Uncertainty in the estimated incident particle track length (if applicable) | $\mu\text{m}$ | Float       |
| EST_PART_THETA     | Estimated incident particle impact angle (if applicable)                    | deg           | Float       |
| EST_PART_THETA_ERR | Uncertainty in the estimated incident particle impact angle (if applicable) | deg           | Float       |

Table 3: Event detection table version v1.0

## 5 Persistence Considerations

### 5.1 Persistence Method(s)

We should describe here the proposed persistence methods (different alternatives file system based or database), with pros and cons.

### 5.2 Size Estimations

Catalog size estimation is a function of :

1. The technology used for the generation of this catalog.
2. The persistence format or system used for storage.

Detection algorithms have been developed and written in Python and the default persistence method adopted is TBD. This results in the following estimations.

**Note:** the following estimations are applicable to catalog version : v1.0

Assuming an average event rate (in the absence of solar activity) of : 5 events/s , the average volume of the catalog per spacecraft revolution is : x bytes. Since Gaia performs 4 full revs on it's spin axis every 24 hrs, the average catalog volume per 24 hrs is : y bytes. This needs then to be multiplied by the total nb of mission days covered by the corresponding version of the catalog.

### 5.3 Long Term Preservation

## 6 Quality Control Metrics

Every run of the batch processing cosmic ray detection algorithms shall generate a new version of the catalog. The corresponding version of the catalog will be quality control checked prior to it's official release.

### 6.1 Internal Consistency Checks

### 6.2 External Consistency Checks

## 7 Catalog Release Mechanism

### 7.1 Catalog Version Generation

The proposed catalog versioning scheme is as follows:

$vN.m$

where

- $N$  is a *major* version of the catalog, only updated due to schema updates (i.e, new attributes added or modifications to existing attributes).
- $m$  is a *minor* version of the catalog updated when a new batch processing is performed **after** algorithmic or software updates.
- executions of a new batch processing with no software or algorithm updates but over an increased mission time range result in the increment of the *minor* version of the catalog.

Every new version of the catalog (major or minor) will be quality control checked prior to it's official release, according to the criteria described in section 6.

### 7.2 Release Mechanism and Notification to Users

This is TBD.

## References

- [1] U. Bastian *Reference Systems, Conventions And Notations for Gaia*.
- [2] R. Kohley *Cosmic rays on BAM CCDs data delivery note*.
- [3] P. G. van Dokkum *Cosmic-Ray Rejection by Laplacian Edge Detection*.
- [4] C. McCully *Astro-SCRAPPY: The Speedy Cosmic Ray Annihilation Package in Python*,  
<https://github.com/astropy/astroscrappy>.